RSC Advances

ROYAL SOCIETY OF CHEMISTRY

www.rsc.org/advances

Effect of sodium doping on microstructure, lattice distortion and magnetic properties of $GdMnO_3$ tiny single crystals

Anshuman Nandy[a], Anirban Roychowdhury[b,c], Tanushree Kar[d], Dipankar Das[b] and Swapan Kumar Pradhan[a,*]

[a]*Department of Physics, The University of Burdwan, Golapbag,Burdwan-713104, India*

[b]*UGC-DAE Consortium for Scientific Research, III/LB-8, Bidhannagar, Kolkata -700098, India*

[c]*Department of Physics, Krishnath College, Berhampore-742101, West Bengal, India*

[d]*Indian Association for Cultivation of Science, Kolkata- 700032, India*

Abstract

Perovskite structured undoped and 10 mol% monovalent Na-doped $GdMnO_3$ compounds are prepared by the sol-gel method. Sintering of these compounds at 1000 ºC for 12h results in formation of well grown, defect-free tiny single crystals of size ~200nm. Detailed microstructural analyses of the compounds are done by Rietveld analysis of XRD patterns. Refined structural and microstructural parameters obtained from Rietveld analysis suggest that Na doping in $GdMnO_3$ reduces the octahedral and Jahn-Teller distortion and increases the structural stability of the compound. EDX analysis confirms the expected composition of the prepared compounds. Microstructure modification due to Na doping is correlated with modification in magnetic ordering. Temperature and magnetic field dependent magnetization measurements reveal the alteration of low temperature magnetic behavior of $GdMnO_3$ on 10mol% Na doping. Mn spin ordering temperature of $GdMnO_3$ increases from 44 K to 51 K after doping. A high coercive field 749 Oe of $GdMnO_3$ and 589 Oe of $Gd_{0.9}Na_{0.1}MnO_3$ at 5 K is

recorded from M-H measurements. Monovalent Na doping in $GdMnO_3$ decreases structural distortion and increases magnetic transition temperature.

* *Corresponding author, e-mail: skpradhan@phys.buruniv.ac.in, Telephone: +91-342-2657800*

Introduction

Perovskite structured rare earth manganates are well studied and vastly used for their excellent magnetic, electrical and magneto-resistive properties.[1-11] $GdMnO_3$ is one of the prime members of the rare earth family due to mid-ionic radius range of Gd and it is an interesting material to study as it posses complex low temperature magnetic ordering as well as ferroelectric ordering.[12-19] Structure and magnetic properties of $GdMnO_3$ ceramics,[16,20-22] in the form of nanoparticles,[12,17,23,24] thin films,[25,26] and single crystals [15, 18, 19, 27-29] had already been studied in details. Like other perovskite manganates, lattice and octahedral distortions are very common in these compounds and their magnetic/electrical properties strongly depend on inherent structural imperfections. The ideal rare earth perovskite manganates possess cubic symmetry with in-built undistorted MnO_6 octahedra.[30] This cubic symmetry is often transformed to tetragonal or orthorhombic due to a change in tolerance factor [9,30] arising from rare earth ions with different ionic radii. This results in lattice distortion and octahedral tilting which affect the structure and properties of the compound to a large extent. Divalent or monovalent doping at rare earth site modifies the microstructure and octahedral distortion in these compounds due to mismatch in ionic radii between rare earth and dopant cations. This leads to changes in the magnetic or electrical behaviors of these compounds. Thus, the magnetic and electrical properties of

$GdMnO_3$ can be tuned depending on the structural changes introduced by dopants at Gd site. Generally, $GdMnO_3$ shows canted anti-ferromagnetic ordering at low temperatures.[16-19] Divalent cation doping at Gd site introduces low temperature ferromagnetic ordering due to Zener double exchange mechanism[31] which is commonly responsible for ferromagnetic behavior in mixed valent manganates.[30] Though the effect of trivalent[32] or divalent cation doping on $GdMnO_3$ were studied[33, 34] well, but studies on monovalent doping are equally interesting. Monovalent cation like Na, K doping on $GdMnO_3$ should have an added advantage over divalent doping as each monovalent cation can convert two Mn^{3+} ions to Mn^{4+} compared to one Mn^{3+} conversion per divalent cation. Thus, monovalent doping should tune the magnetic properties more effectively than divalent doping. To the best of our knowledge, monovalent cation doping on $GdMnO_3$ has not been studied earlier. Thus, a detailed structural analysis is a prime necessity to understand the modification in lattice or octahedral distortion of $GdMnO_3$ due to monovalent doping because of the changes in crystal structure and microstructure parameters. In this work, we have studied the effect of 10mol% Na doping on microstructure and magnetic properties of $GdMnO_3$ compounds because Gd is in the mid-ionic radius range in the rare earth family and possess large spin-only magnetic moment ($7.94\mu_B$). Na is chosen as monovalent dopant as ionic radii of Na^{+1} and Gd^{3+} are very close and mismatch of ionic radii between dopant and parent ions would be less, which is always desirable from the stability point of view of the compound. Doping level is chosen as 10mol% as it would convert 20mol% Mn^{+3} to Mn^{+4} which should influence ferromagnetic behavior of the compound without significant structural changes. The primary objective of the present work is to elucidate the effect of monovalent dopant on structure and magnetic properties of $GdMnO_3$ compounds which is not reported yet to a noticeable extent.

Experimental section

Materials and methods

$GdMnO_3$ and $Gd_{0.9}Na_{0.1}MnO_3$ compounds are synthesized by simple and conventional sol-gel route. For preparation of $GdMnO_3$ compound, Gadolinium Oxide (Gd_2O_3, SRL, >99%) and Manganese (II) acetate tetrahydrate ($(CH_3COO)_2Mn.4H_2O$, MERCK, >99.5%) were taken in stoichiometric ratio and transformed into nitrates by adding concentrated Nitric acid. The nitrates were then mixed and the mixture was heated at 100ºC for 30 minutes. Water solution of stoichiometric citric acid was then added to the mixture. Ethylene Glycol was added drop wise to the mixture after 30 minutes and the mixture was stirred for 2 hours. Then the mixture was kept at 100ºC for 8 hours and a homogeneous gel was formed which was later fired at 200ºC to get a brownish powder. The same preparation route was followed earlier by our group.[35] To prepare $Gd_{0.9}Na_{0.1}MnO_3$, 10 mol% of Gd_2O_3 was replaced by equivalent amount of Sodium Carbonate (Na_2CO_3, purity, MERCK) and the entire synthesis procedure was repeated. Sintering of both undoped and doped compounds was carried out in steps at 400º, 600º, 800º and finally at 1000ºC for 12 h to get pure single phase and well crystalline compounds. All samples were furnace-cooled to room temperature with very slow rate of cooling and then collected for characterizations.

Characterization techniques and method of analysis

X-ray diffraction (XRD) patterns of the annealed samples were recorded with D8 Advanced diffractometer (Bruker, Da Vinci model) using CuK_α radiation in step scan mode (step size: 0.02º, counting time: 2sec/step) for the angular range 20º- 80º2θ. Transmission electron micrographs were studied from a high resolution transmission electron microscope (HRTEM)

(JEOL-JEM 2010) operated at 200 KV. Compositional analyses were carried out by Energy dispersive X-ray (EDX) spectroscopy available with TEM facility. The dc magnetization under varying temperature and field were recorded by a superconducting quantum interference device (SQUID) magnetometer (MPMS XL 7, Quantum Design, USA). The temperature dependent magnetization (M-T) was recorded in the temperature range of 5K to 300K in zero-field-cooled (ZFC) and field-cooled (FC) conditions under a constant magnetic field 500 Oe. The field dependent magnetization was recorded in a field variation ±30kOe at 5K temperature.

The detailed microstructural characterization of the prepared compounds was accomplished by analyzing respective XRD patterns by Rietveld structure and microstructure refinement method using MAUD software version 2.26.[36-40] The design of MAUD software is previously discussed and its usefulness in microstructural analysis is already established.[36] The observed X-ray powder diffraction pattern was simulated with the phases obtained from ICSD database by the Marquardt least-squares procedure which minimizes the difference between the observed and simulated powder diffraction patterns. This minimization was monitored using the reliability index parameter, R_{wp} (weighted residual error) and R_{exp} (expected error) defined respectively as,

$$R_{wp}= \left[\frac{\sum_i w_i\left(I_0 - I_c\right)^2}{\sum_i w_i\left(I_0\right)^2}\right]^{1/2}$$

$$R_{exp}= \left[\frac{(N-P)}{\sum_i w_i\left(I_0\right)^2}\right]^{1/2}$$

where I_0 and I_C are the experimental and calculated intensities, w_i (=$1/I_0$) and N are the weight and number of experimental observations and P the number of fitting parameters. This leads to the value of goodness of fit (GoF):

$$\text{GoF} = \frac{R_{wp}}{R_{exp}}$$

HRTEM images were analyzed by ImageJ software. Atomic level diagrams are prepared by ATOM software version 6.2 using Rietveld refinement outputs.

Results and discussion

Microstructural Studies

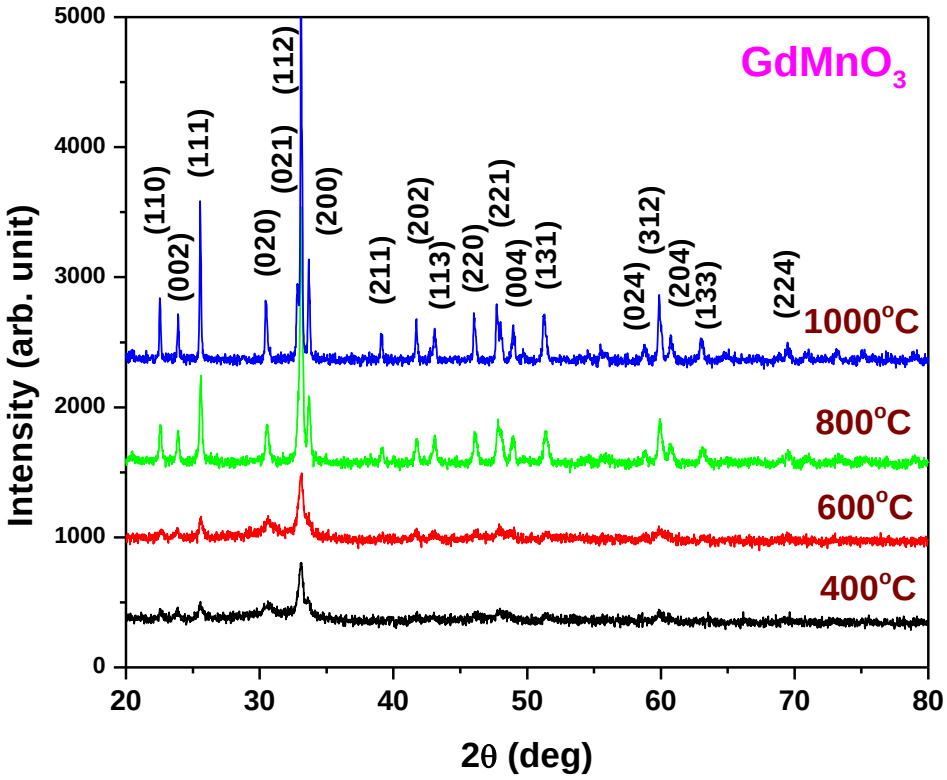

Fig. 1. Powder x-ray diffraction patterns of $GdMnO_3$ compound sintered at different temperatures.

X-ray powder diffraction patterns of $GdMnO_3$ compound sintered at different temperatures are shown in Fig. 1. XRD patterns are recorded after each heat treatment of the compound at 400ºC, 600ºC, 800ºC and 1000ºC. It is clearly evident that the compound has been formed with single phase just after heat treatment of the dried gel at 400ºC for 12h, but due to small crystallite size all reflections are significantly broadened and as a result most of the reflections are not resolved due to high degree of peak overlapping. With increase in heat treatment temperature up to 600ºC there is no noticeable change in XRD pattern. After sintering compound at 800ºC remarkable change in XRD pattern has been evidenced. All reflections of the compound have been well resolved due to significant reduction in peak broadening resulting primarily from increase in crystallite size with increase in sintering temperature. Final sintering at 1000ºC results in complete growth of well crystalline single phase $GdMnO_3$ compound in which well resolved reflections appear with accurate relative intensity ratio as per the ICSD file # 157393[27] and all reflections are indexed accordingly. It is to be noted that there is no trace of any other reflection in any of the XRD pattern, which signify that the pure $GdMnO_3$ has been synthesized at 400ºC and with increase in sintering temperature crystallite size of compound increase apparently without any phase transition up to 1000ºC.

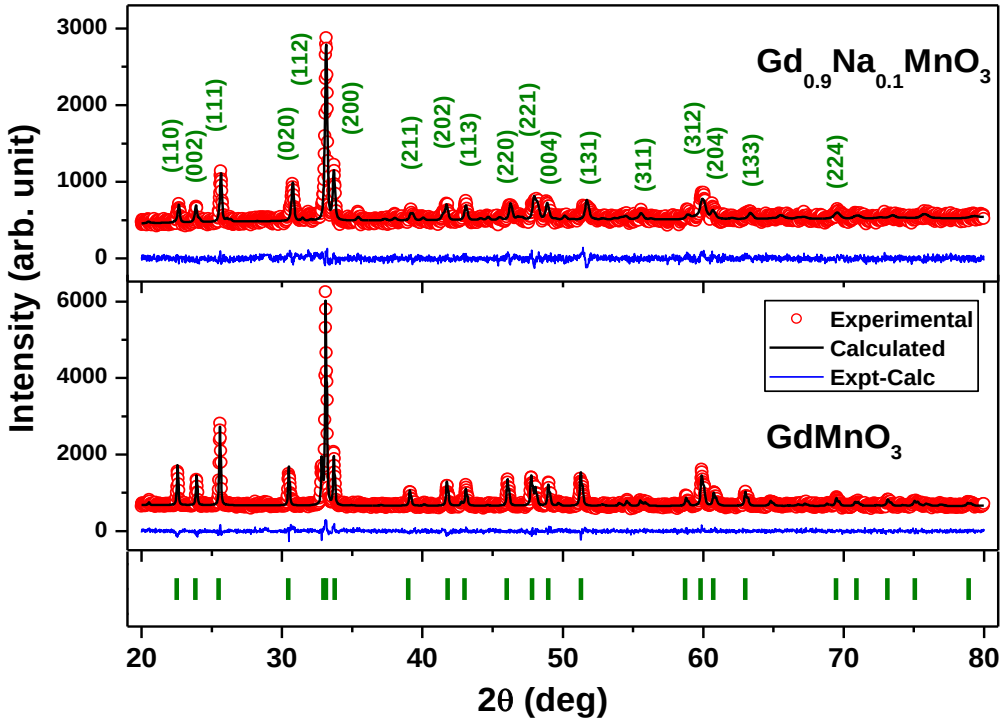

Fig. 2. Experimental (o) and Rietveld refined (-) XRD patterns along with the difference between experimental and refined pattern of $GdMnO_3$ (lower panel) and $Gd_{0.9}Na_{0.1}MnO_3$ compounds. Markers show peak positions.

XRD patterns of $GdMnO_3$ and $Gd_{0.9}Na_{0.1}MnO_3$ compounds along with their Rietveld refined outputs are shown in Fig. 2. Both these compounds are found to crystallize in orthorhombic unit cell with P_{bnm} space group. XRD patterns of these compounds are simulated with the structural information available in the ICSD file # 157393[27]. In case of Na-doped compound, 10mol% Gd has been substituted by equal amount of Na. Refinements of structural and microstructural parameters continued till the GoF approaches very close to 1.0 (range of GoF varies between 1.175 and 1.227), signifies that fitting quality of these XRD patterns are quite good. The intensity differences between experimental and refined XRD patterns are insignificant and shown at the bottom of the respective patterns. All structural and microstructure

parameters revealed from the Rietveld refinement are tabulated in Table 1. Lattice parameters of orthorhombic $GdMnO_3$ and Na-doped compounds are very close to the reported ICSD values and follow the relation $\frac{c}{\sqrt{2}}$<**a**<**b**. It confirms both these compounds are in O´ orthorhombic structure[41] composed of distorted MnO_6 octahedra formed due to strong co-operative Jahn-Teller effect. Lattice parameters **a** and **b** of Na-doped compound are reduced whereas **c** is expanded in comparison to the undoped one and overall there is a lattice contraction due to Na doping, which indicates towards formation of a more symmetrical structure in Na-doped compound. Though ionic radius of Na^+ (1.24 Å) is greater than Gd^{3+}(1.107Å),[42] the unit cell volume is less for $Gd_{0.9}Na_{0.1}MnO_3$ as substitution of trivalent Gd by monovalent Na results in shortening of Mn-O bonds. A 9 co-ordination approach is considered here for more accurate value of ionic radius of smaller lanthanide Gd in perovskite unit cell.[41] The decrease in difference between two lattice parameters ($|a-b|$) and unit cell volume in $Gd_{0.9}Na_{0.1}MnO_3$ also indicates that the Na-doped compound is more symmetrical. The perovskite lattice parameter (a_P) is calculated and given in Table 1. Lattice parameters of orthorhombic perovskite structure relate to cubic lattice parameter (a_P) of the ideal perovskite as $\mathbf{a_P} = \frac{V^{1/3}}{2}$ where V is the unit cell volume. a_P is reduced after Na doping as the ionic radii of Mn^{4+} present in the Na doped compound is smaller than Mn^{3+}.[43] A decrease in spontaneous strain (s) due to 10mol% Na doping also indicates a decrease in lattice distortion.[41] Particle size and r.m.s lattice strain are also calculated for both compounds by Rietveld refinement and shown in Table 1. Na-doped compound with smaller particle size contains less lattice strain in comparison to undoped compound. Changes of other structural parameters like fractional coordinates and atomic occupancies are presented in Table 1. Changes in magnetic properties of $GdMnO_3$ due to microstructural changes introduced by Na-doping are discussed in later section.

Table 1 Calculated structural and microstructural parameters of undoped and Na-doped $GdMnO_3$ compounds revealed from the Rietveld structure and microstructure refinement.

Parameters	**ICSD #157393**	**$GdMnO_3$**	**$Gd_{0.9}Na_{0.1}MnO_3$**
R_w		4.314	5.238
R_{exp}		3.670	4.269
GoF		1.175	1.227
a (Å)	5.3160	5.3184(06)	5.3160(28)
b (Å)	5.8683	5.8622(77)	5.8045(44)
c (Å)	7.4252	7.4372(18)	7.4464(76)
(| a-b |) (Å)	0.5523	0.5438	0.4885
Cell Volume (V)	231.636	231.877	229.774
Perovskite parameter (a_p)	3.0707	3.0718	3.0625
Spontaneous strain (s)		0.097	0.088
Particle size (nm)		169.70(8)	157.63(9)
Microstrain ($\times 10^{-4}$)		2.12(4)	1.44(0)
Gd/ Na: (x, y, 0.25) Occupancy ⟶		0.984(1)	0.881(3)/ 0.112(4)
x	0.9802	0.9858(9)	0.9834(4)
y	0.0818	0.0791(2)	0.0866(1)
Mn: (0.5, 0, 0) Occupancy ⟶		1.019(4)	1.015(4)
O1: (x, y, 0.25) Occupancy ⟶		1.012(1)	1.012(2)
x	0.1067	0.1003(2)	0.0916(0)
y	0.4649	0.4675(6)	0.5245(7)
O2: (x, y, z) Occupancy ⟶		1.010(0)	1.015(7)
x	0.7236	0.7205(9)	0.6779(6)
y	0.3179	0.3145(2)	0.2831(2)

z	0.0495	0.0508(5)	0.0447(4)

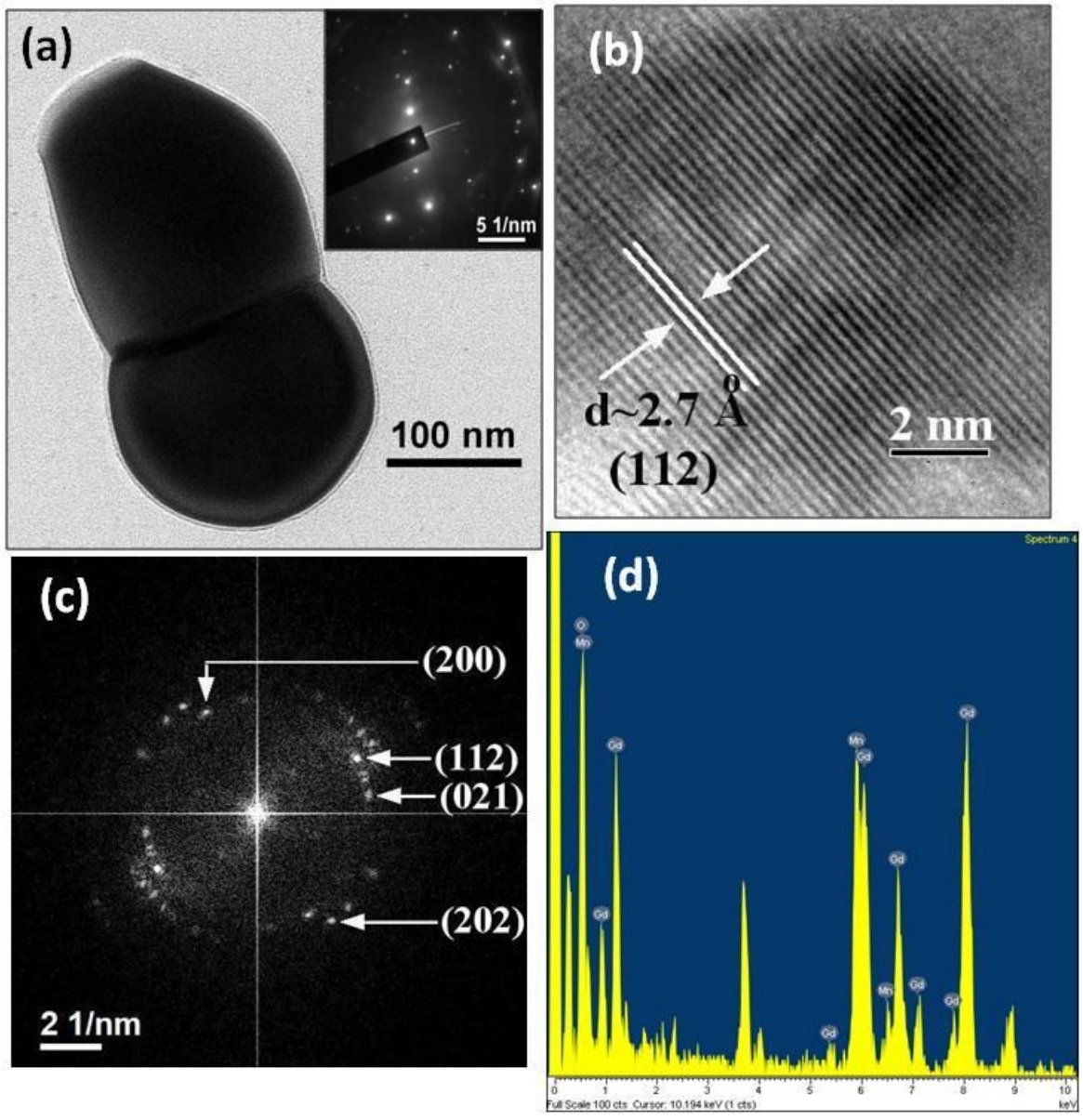

Fig. 3. HRTEM images of $GdMnO_3$: (a) two overlapping tiny single crystals [inset: single crystal diffraction spots obtained from TEM], (b) lattice fringe pattern (c) FFT pattern (d) TEM-EDX spectra.

To see the nature of crystallinity of $GdMnO_3$ compound some TEM images are taken and are presented in Fig. 3. It is interesting to note that the compound is composed of well grown tiny single crystals of about ~200nm length (Fig. 3a), which is very close to crystallite size obtained

from the Rietveld refinement (Table 1). A portion of such a single crystal is imaged under HRTEM and the fringe pattern [Fig. 3b] affirms the fault free growth of most dense (112) lattice planes of the compound. As these grains are quite large than the electron beam aperture at the operating voltage of TEM, the SAED powder diffraction ring pattern could not be recorded. However, the fast fourier transformed (FFT) pattern [Fig. 3c] has been indexed with some distinct reflections of the compound by comparing the spot distances with the corresponding d-values for the reflecting planes. Compositional analysis of the compound has been estimated from the TEM-EDX spectra, shown in Fig. 3d and elemental contents both in wt% and at% are tabulated in Table 2. Respective at% of the elements in the compound are well in accordance with the expected composition. Fig. 4 shows the HRTEM images of $Gd_{0.9}Na_{0.1}MnO_3$ compound and also indicates the well crystalline nature of the sample. Some of the tiny single crystals are shown in Fig. 4a. It may be noted that average size of these irregular shaped tiny single crystals is smaller than that obtained from Rietveld refinement, because of the fact that during TEM sample preparation by crushing powder sample, tiny single crystals were further broken into smaller irregular pieces. The fringe pattern [Fig. 4b] affirms the presence of two most intense (111) and (112) reflecting planes of the Na-doped compound and like the undoped compound there is no planar imperfection in the doped compound. Some of the most intense reflections of the compound have been identified and indexed in the FFT pattern [Fig. 4c] taken from the assemblage of tiny single crystals. TEM-EDX spectra of the compound shown in Fig. 4d have been considered for the elemental composition analysis and presented in Table 2. Content of the elements in at% are close to the expected composition of the Na-doped compound.

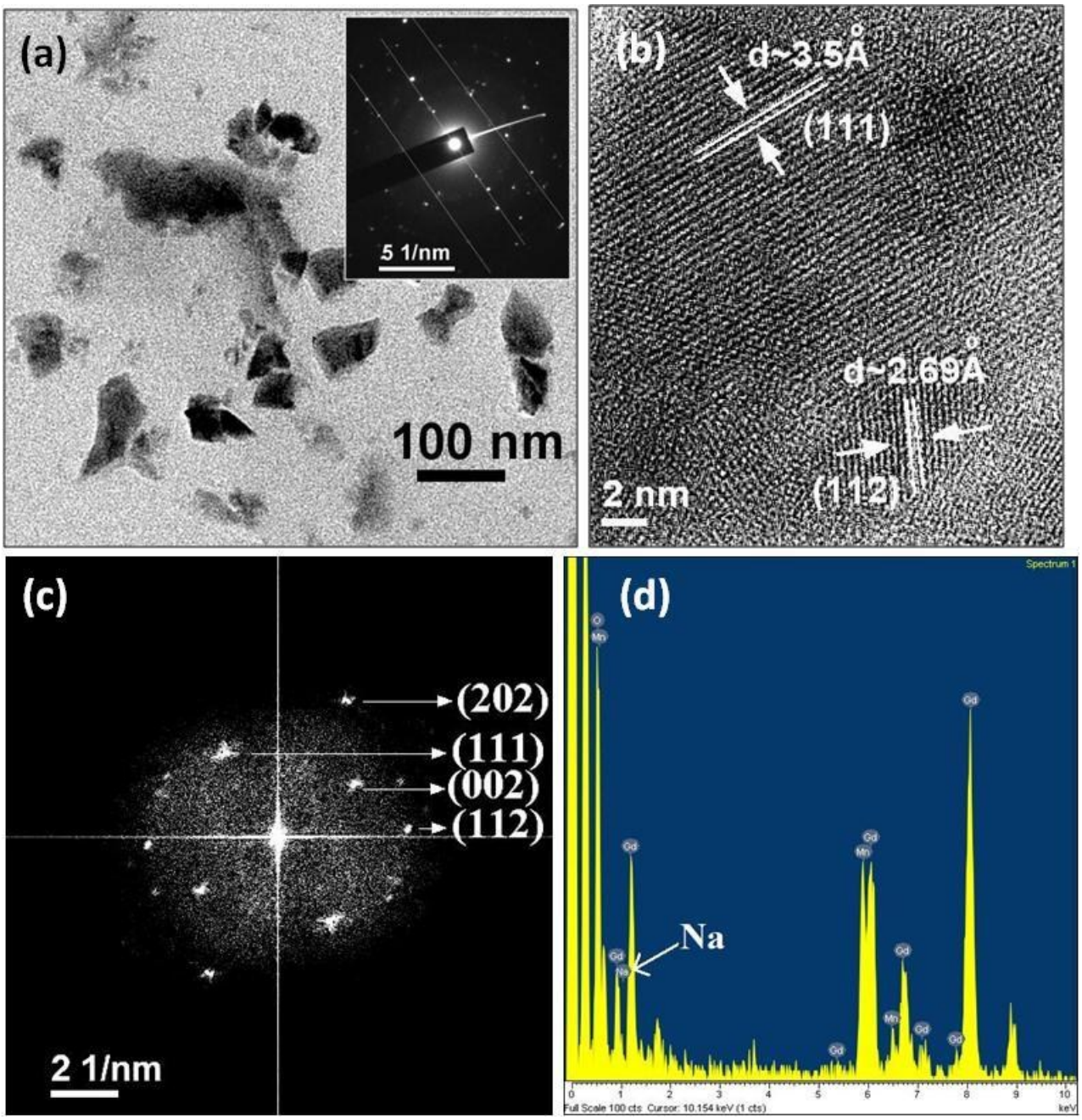

Fig. 4. HRTEM images of $Gd_{0.9}Na_{0.1}MnO_3$: (a) some tiny single crystals [inset: single crystal diffraction spots obtained from TEM] (b) lattice fringe pattern (c) FFT pattern (d) TEM-EDX spectra.

Table 2 Elemental composition analyses of undoped and Na-doped $GdMnO_3$ compounds estimated from respective TEM-EDX spectra.

Sample	Element	Weight%	Atomic%
$GdMnO_3$	O K	20.04	62.72
	Mn K	19.94	18.17
	Gd L	60.02	19.11
$Gd_{0.9}Na_{0.1}MnO_3$	O K	26.03	70.01
	Na K	0.72	1.34
	Mn K	16.87	13.21
	Gd L	56.38	15.43

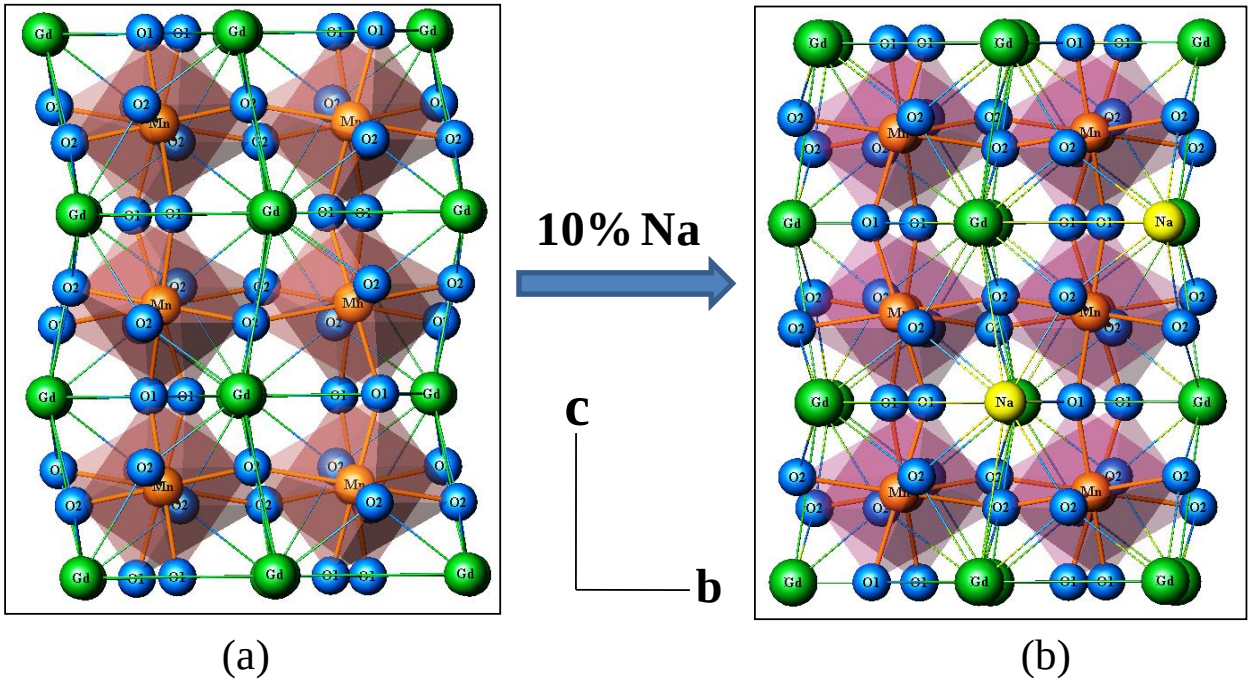

Fig. 5. Atomic level representation of (a) $GdMnO_3$ (b) $Gd_{0.9}Na_{0.1}MnO_3$.

Schematic atomic level diagrams of $GdMnO_3$ and $Gd_{0.9}Na_{0.1}MnO_3$ generated based on the refined structural parameters revealed from Rietveld analysis of respective XRD patterns are shown in Fig. 5. In undoped compound Gd^{3+}, Mn^{3+} and O^{2-} ions occupy corner, body centre and face centre positions of the perovskite lattice respectively (Fig. 5a). In Na-doped compound, 10mol% Na^{+} substitutes only the equivalent amount of Gd^{3+} without much disturbing other ionic positions of the lattice. Six face centered oxygen atoms form MnO_6 octahedra which is the basic building block of these compounds. The perovskite structure in manganates is influenced by two types of distortions: (i) from co-operative tilting of MnO_6 octahedra and (ii) due to Jahn Teller effect of Mn^{+3}.[9] The distortion due to tilting of the octahedra originates from the mismatch of ionic radii of the cations and anions present in the lattice. It is governed by Goldschmidt tolerance factor given by

$$\mathbf{t} = \frac{<r_A>+r_O}{\sqrt{2}(<r_B>+ r_O)} = \frac{d_{A-O}}{\sqrt{2}(d_{Mn-O})}$$

The average A site radius in ABO_3 compound increases due to Na doping in place of Gd as ionic radius of Na^{+} is greater than Gd^{3+}. The Goldschmidt tolerance factors are calculated for both undoped and Na-doped compounds based on these parameters listed in Table 3.

Table 3. Different bond angles and bond lengths of undoped and Na-doped $GdMnO_3$ compounds obtained from the Rietveld structure refinements of respective XRD patterns.

Bond Angles ↓	**$GdMnO_3$**	**$Gd_{0.9}Na_{0.1}MnO_3$**
Mn-O1-Mn (×2)	146.1	149.5
Mn-O2-Mn (×4)	149.9	149.7
$<\cos^2\theta>$	0.7286	0.7444
$<\omega>$	31.37	30.37

Bond Lengths (Å) ↓		
Mn-O1 (×2)	1.94	1.95
Mn-O2 (×2)	1.88	1.87
Mn-O2 (×2)	2.22	2.20
$<Mn-O>_a$	2.013	2.007
Gd-O1	2.36	2.69
Gd-O1	2.30	2.19
Gd-O2 (×2)	2.64	2.53
Gd-O2 (×2)	2.47	2.51
Gd-O2 (×2)	2.41	2.49
$<Gd-O>_a$	2.462	2.492
$t_9 = d_{Gd-O}/\sqrt{2}d_{Mn-O}$	0.8650	0.8782

It is evident from Table 3 that the calculated tolerance factor (t) is higher in Na-doped compound, which indicates a less distortion and better stabilization in Na-doped $GdMnO_3$. The average angular distortion of MnO_6 octahedra can be calculated from <Mn-O-Mn> bond angle <θ> as <ω> = 180º-<θ>. The change in bond angles due to Na doping is shown in Fig. 6 and <ω> values are listed in Table 3. The decrease in difference of lattice parameters **(|a-b|)** [Table 1] in Na-doped compound implies that the octahedral tilting should be less and Mn-O-Mn bond angle should be closer to 180º.[19] It has been verified from the measured values of Mn-O-Mn bond angles. The angular distortion reduced due to Na doping and thus a more stable MnO_6 octahedra forms by monovalent doping. An increase in 't' with a decrease in <ω> again establishes the well known fact that magnitude of octahedral tilting in perovskites is qualitatively

related to the tolerance factor.[41, 44] Though the O-Mn-O bond angles are 180º, the individual O1-Mn-O1 and O2-Mn-O2 bond angles differ from 90º. This is shown in Fig. 7 and it signifies presence of distortion within a single MnO_6 octahedron.[45] The change in Mn-O-Mn and O-Mn-O bond angles due to doping should influence the magnetic properties in the doped compound.

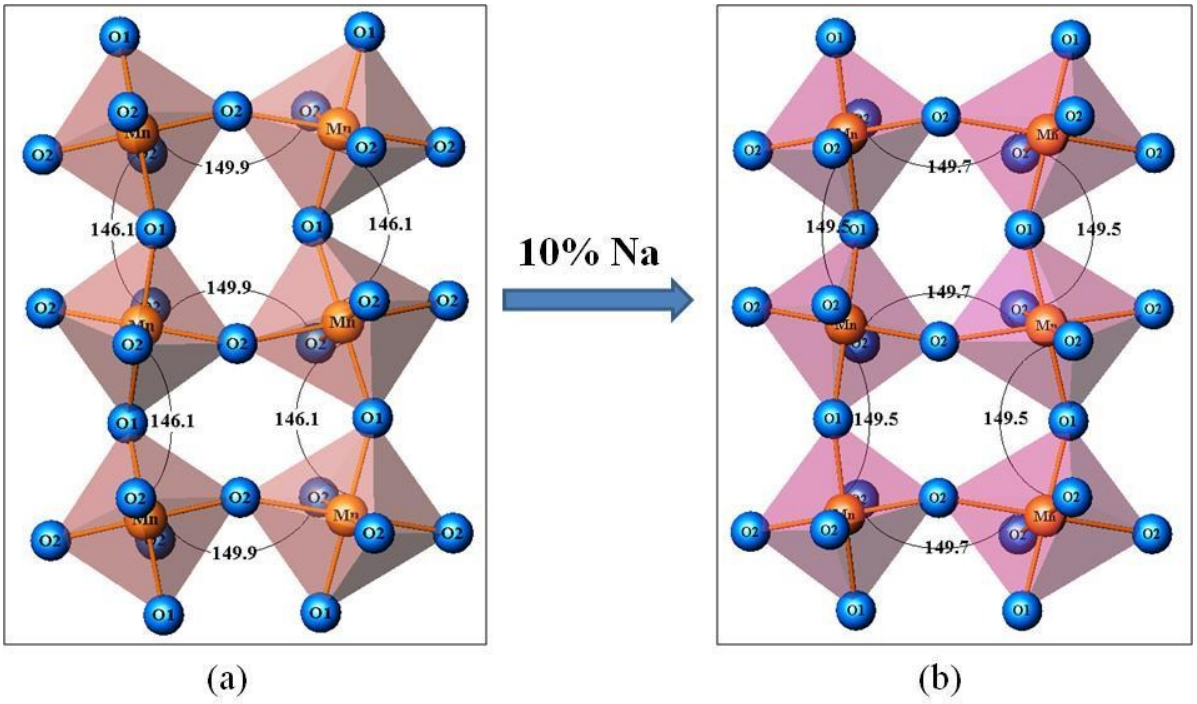

Fig. 6. Mn-O-Mn bond angles in (a) $GdMnO_3$ and (b) $Gd_{0.9}Na_{0.1}MnO_3$ compounds.

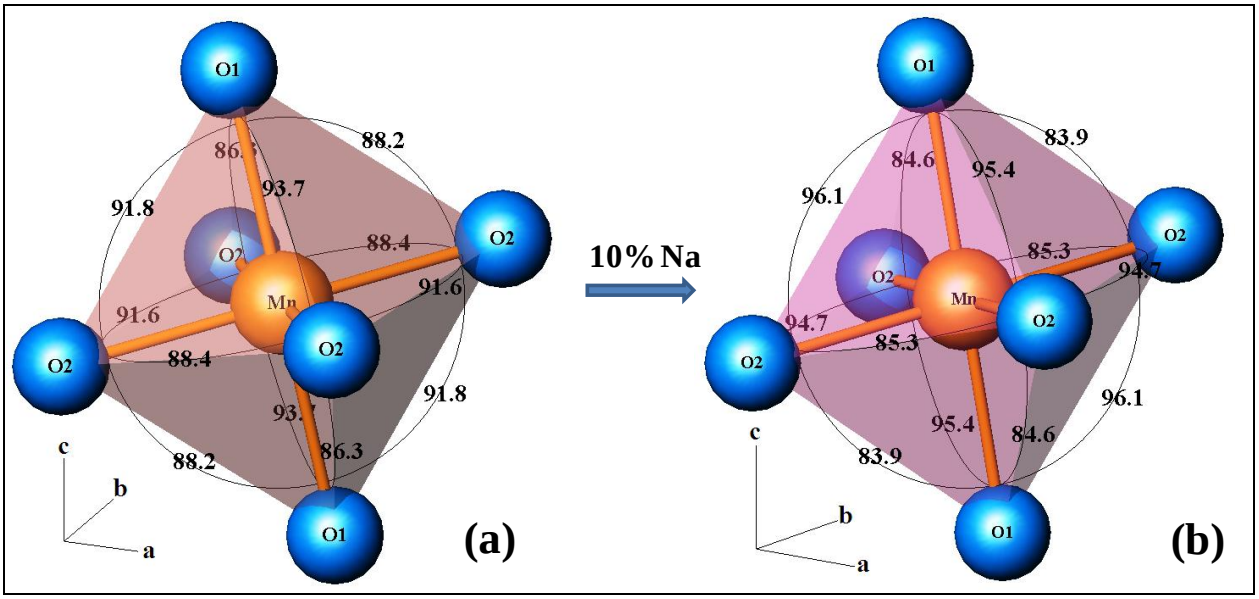

Fig. 7. O-Mn-O bond angles in (a) $GdMnO_3$ and (b) $Gd_{0.9}Na_{0.1}MnO_3$ compounds.

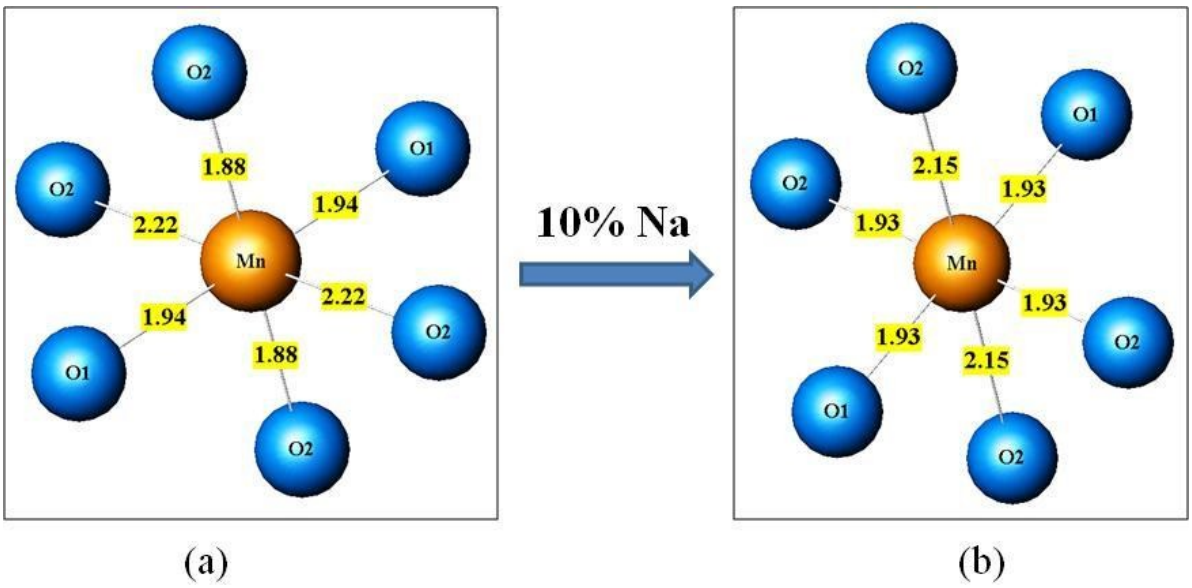

Fig. 8: Mn-O bond lengths of (a) $GdMnO_3$ and (b) $Gd_{0.9}Na_{0.1}MnO_3$ compounds.

Due to the Jahn-Teller distortion, MnO_6 octahedra is distorted in such a way that there is mismatch in Mn-O bond lengths. The change in Mn-O bond lengths after doping is shown in Fig. 8 and listed in Table 3 along with Gd-O bond lengths. The charge imbalance introduced by 10mol% replacement of Gd^{3+} by Na^{+} results into 20% conversion of larger Mn^{3+} ions (0.58Å)

into smaller Mn^{4+} ions (0.53Å) which maintains the charge neutrality in the doped compound. The decrease in Mn-O bond lengths is also associated with the conversion of valence state Mn atom present at the centre of 6 co-ordinated MnO_6 octahedron. This replacement of Jahn-Teller (JT) Mn^{3+} ions [43] by non-JT Mn^{4+} ions reduces the lattice distortion in $Gd_{0.9}Na_{0.1}MnO_3$ and makes it more symmetrical and thereby less distorted than the undoped compound. The existence of Mn^{4+} ions in $Gd_{0.9}Na_{0.1}MnO_3$ compound is confirmed by the presence of Mn $2p_{3/2}$ XPS spectra as shown in Fig. 9. The asymmetrical peak in the XPS spectra is fitted with two Gaussian peaks at 641.2 eV and 642.7 eV corresponding to the binding energies of Mn^{3+} and Mn^{4+} respectively.

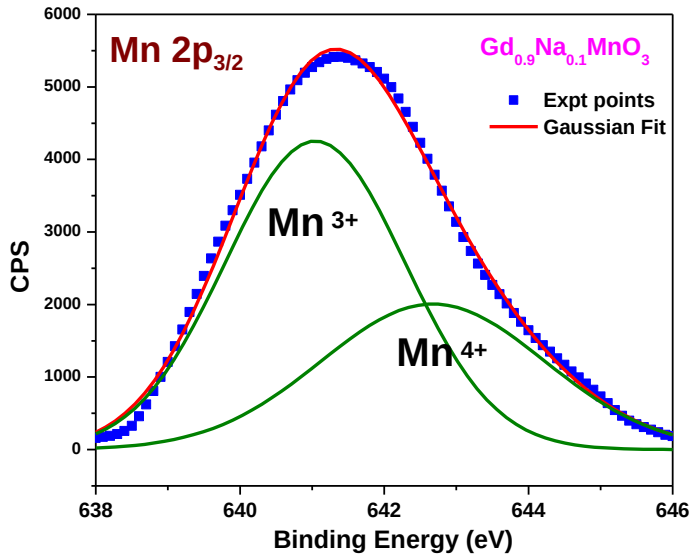

Fig. 9. The XPS spectra Mn $2p_{3/2}$ fitted with two Gaussian peaks.

Magnetic properties of undoped and Na-doped $GdMnO_3$ compounds

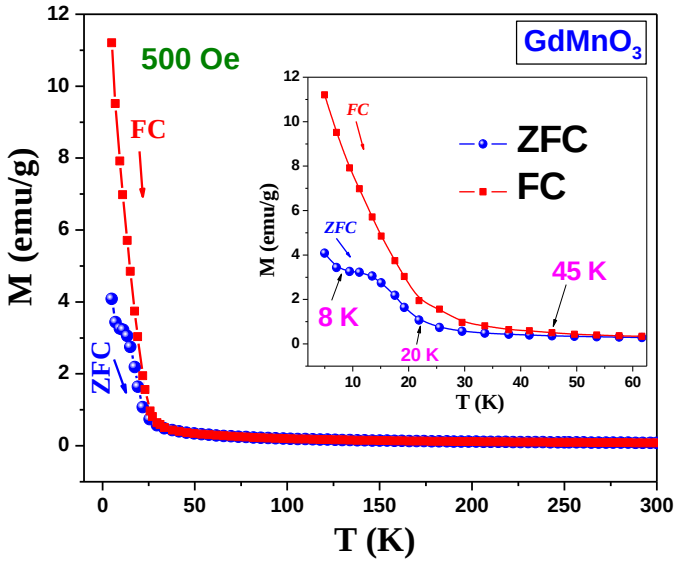

Fig. 10.Temperature dependent zero field cooled (ZFC) and field cooled (FC) magnetization curves of $GdMnO_3$ compound. Inset shows the enlarged part of low temperature region.

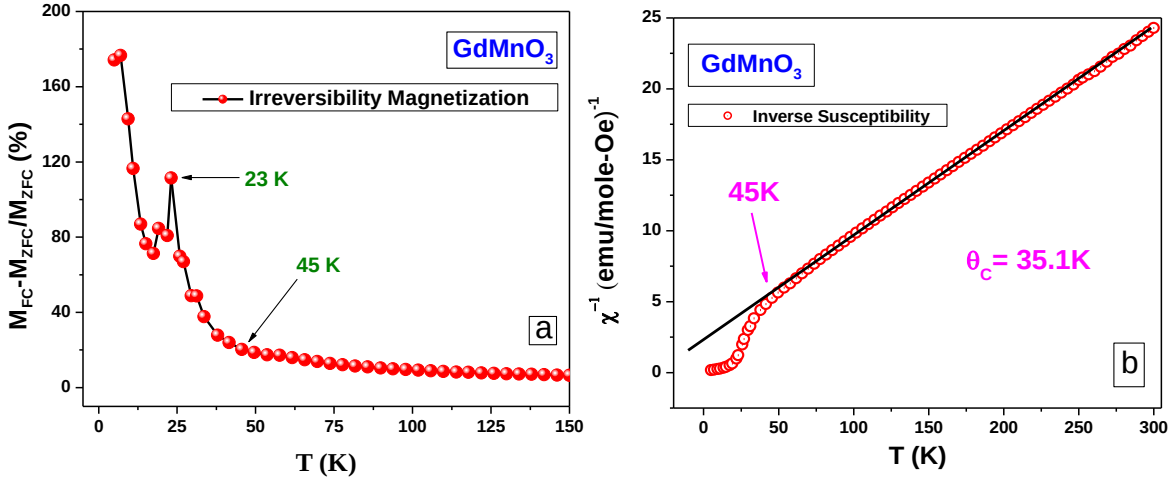

Fig. 11. Temperature dependent (a) Irreversibility magnetization and (b) Inverse susceptibility of $GdMnO_3$ single crystals.

Fig. 10 shows the temperature dependent magnetization curves of $GdMnO_3$ compound in zero-field-cooled (ZFC) and field-cooled (FC) conditions, recorded at 500 Oe constant magnetic field. The compound is paramagnetic (PM) at room temperature and shows complex magnetic properties below ~50K. The magnetic structure of $GdMnO_3$ compound comprises of a negative exchange interaction between two magnetic sub-lattices: a ferromagnetic (FM) Mn sublattice and an anti-ferromagnetically (AFM) ordered Gd sublattice.[19, 22] In this compound, the Mn-Mn coupling is much stronger than Mn-Gd and Gd-Gd coupling due to stronger 3d exchange interaction than 4f.[46] The Gd magnetic moments are oppositely ordered by the internal field created by Mn spins.[22] Three anomalies in the ZFC curve can be seen on warming after a ZFC procedure as the FM in-plane interaction between canted Mn-spins in the ab plane compete with the AFM inter-planar interactions along c-axis.[19, 22] The first minute change in the ZFC curve with lowering of temperature can be seen at 45K. This temperature can be attributed as the Nèel temperature of transition to an incommensurate AFM (ICAFM) phase due to ordering of Mn^{3+} moments in $GdMnO_3$.[15] Earlier, similar behavior was also seen for $GdMnO_3$ compound at 42 K,[16] for nanoparticles at 44K,[17] for bulk ceramics at 40K [20] and for thin films at 42K.[25] Further, a broad bump in ZFC curve is observed below 20K which arises from canted A-type AFM (c-AFM) ordering associated with a weak ferromagnetism due to canted Mn^{3+} spin ordering and Gd 4f spin polarization.[16-19] Thus, the ICAFM to c-AFM transition temperature is noted at 20K. The third anomaly in ZFC curve can be observed at 8K. This temperature can be attributed to the onset of an AFM long range ordering of Gd magnetic moments, as also reported in previous studies.[16, 17, 19] After a field cooling measurement, the magnetization increases and the low temperature anomalies in magnetization disappears due to the enhancement of local field at Gd positions arising from ferromagnetic ordering of Mn moments.

Fig. 11a illustrates the temperature dependent irreversibility magnetization which depicts the amount of bifurcation between ZFC and FC magnetizations. A large bifurcation between ZFC and FC curves starts appearing below the Neel temperature 45K which continuously increases with lowering of temperature to as high as 180%. This large bifurcation is a signature of magnetic anisotropy in the compound arising from competing weak ferromagnetic and anti-ferromagnetic behavior and presence of spin glass like phase.[35, 47] Structural anisotropy also may be a reason of magnetic anisotropy. This Fig. also shows that ICAFM and c-AFM regions are divided by a peak. Fig. 11b shows the inverse susceptibility by dots and Curie law fit by solid line through these dots. Experimental data points deviates from theoretical fit below 45K due to transition from PM to c-AFM stage. Another change in nature of slope is observed at 20K which signifies the c-AFM to ICAFM phase transition at 20K as discussed from ZFC curve. The calculated Curie-Weiss temperature θ_C is 35.1K which is little less than the temperature for Mn ordering 45K. Value of θ_C is in good agreement with previous report.[16] The calculated effective magnetic moment is also close to the theoretical value.

Field dependent magnetic hysteresis curve of $GdMnO_3$ taken at 5K is shown in Fig. 12. Extracted coercive field is found to be 749.2Oe and the unsaturated magnetization at high field indicates the presence of canted antiferromagnetic states. The remnant magnetization value is same as the FC magnetization value in the long range ordering stage of Gd moments which signifies that the magnetic moment at 5K is due to Gd spin ordering only. The high coercivity value is due to the aligned Gd spins in the external magnetic field.

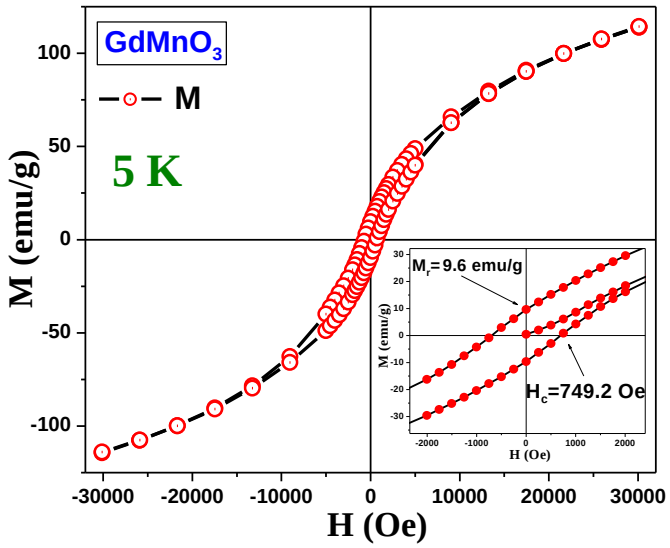

Fig. 12. M-H loop of $GdMnO_3$ compound taken at 5K. Inset shows the enlarged hysteresis part of the loop.

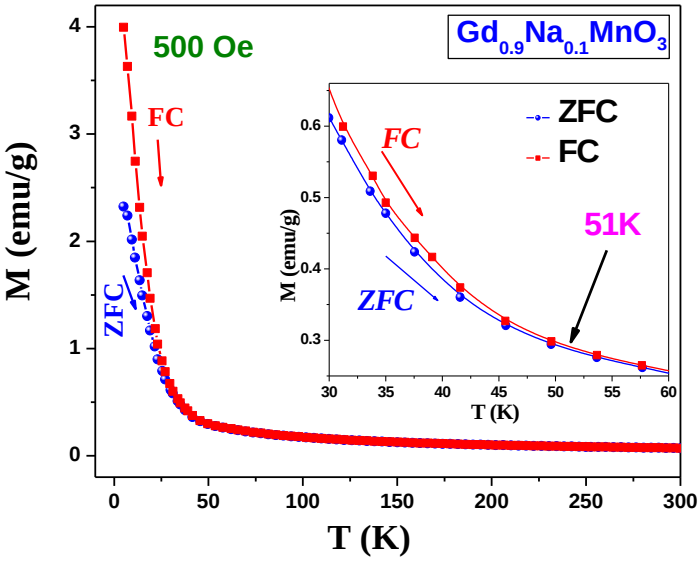

Fig. 13. Temperature dependent zero field cooled (ZFC) and field cooled (FC) magnetization curves of $Gd_{0.9}Na_{0.1}MnO_3$ single crystals. Inset shows the enlarged part of low temperature region.

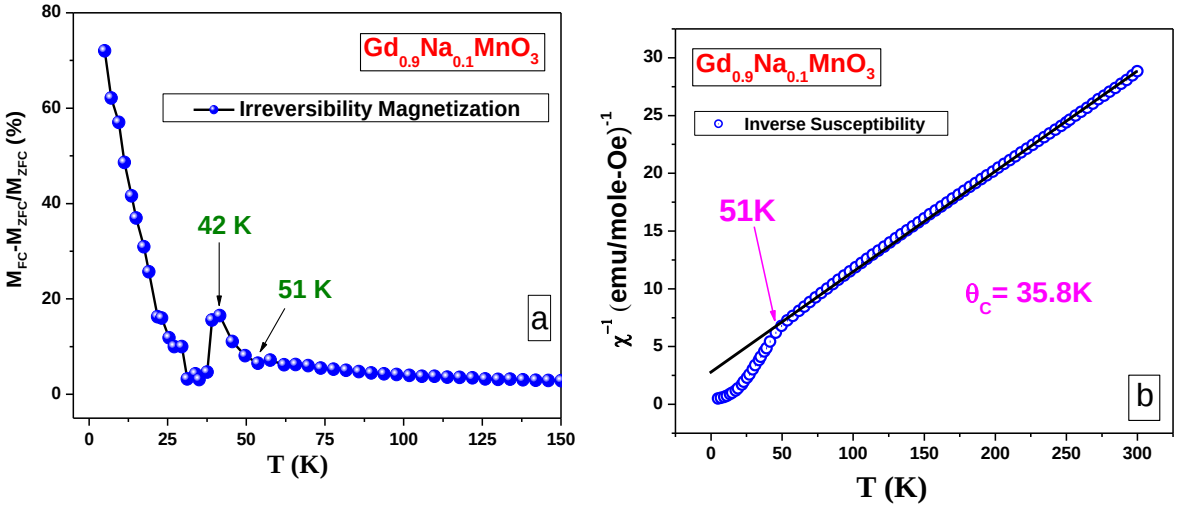

Fig. 14. Temperature dependent (a) Irreversibility magnetization and (b) Inverse susceptibility of $Gd_{0.9}Na_{0.1}MnO_3$ compound.

An increase in magnetic transition temperature with increase in tolerance factor is expected for divalent doping to rare earth perovskites at low temperature range [10, 30, 48] and the similar finding is also expected in the present case with monovalent Na doping in $GdMnO_3$ compound. An increase in Mn-O-Mn bond angle towards 180º due to doping strengthens the FM interaction within ab planes but does alter the AFM coupling along c-axis which in turn increases the Curie temperature.[19] Temperature dependent magnetization curves for $Gd_{0.9}Na_{0.1}MnO_3$ are shown in Fig. 13. Magnetic behavior of this compound is different as in addition to the negative exchange interaction between the ferromagnetically aligned ab planes, ferromagnetic double exchange (DE) interaction between Mn^{+3}-O^{-2}-Mn^{+4} networks [31] appears in

the system due to inclusion of Mn^{+4} ions in the system. Though the canted AFM structure is still present in the compound, Na doping shifts the Mn spin alignment temperature to a higher value due to this DE interaction. The Mn spin ordering temperature or the Curie temperature is noted as 51K. Lower to this temperature, the anomaly near 20K cannot be observed from the ZFC curve as the stronger ferromagnetic double exchange interaction suppresses the ICAFM to c-AFM phase transition. Long range AFM spin ordering of Gd starts below 7K.

The bifurcation between ZFC and FC curves is shown in Fig. 14a and it shows a maximum 72% bifurcation, much less than that in the undoped $GdMnO_3$. A decrease in bifurcation also points to the fact that competing AFM interaction is less in the Na-doped compound. Also the structural anisotropy in the Na-doped compound is less which in turn lowers the magnetic anisotropy. Curie law fit is shown in Fig. 14b where a deviation from Curie law fit (solid line) can be seen at 51K similar to as found in the magnetization curve. The Curie Weiss temperature θ_C is calculated as 35.8K which is less than actual T_C. The effective magnetic moment, as expected, is less than that of the undoped compound. This temperature is already attributed to Mn spin ordering temperature from the ZFC curve.

Hysteresis curve of $Gd_{0.9}Na_{0.1}MnO_3$ at 5K is shown in Fig. 15 and the coercive field is measured as 589.2Oe. The remnant magnetization value at 5K is same as the FC moment at 5K which again signifies that at this temperature the Gd spin ordering plays the dominant role. The coercive field is still high but is less than that of the undoped compound as 10mol% magnetic Gd^{3+} ions are replaced by non-magnetic Na^{+} ions in the doped compound.

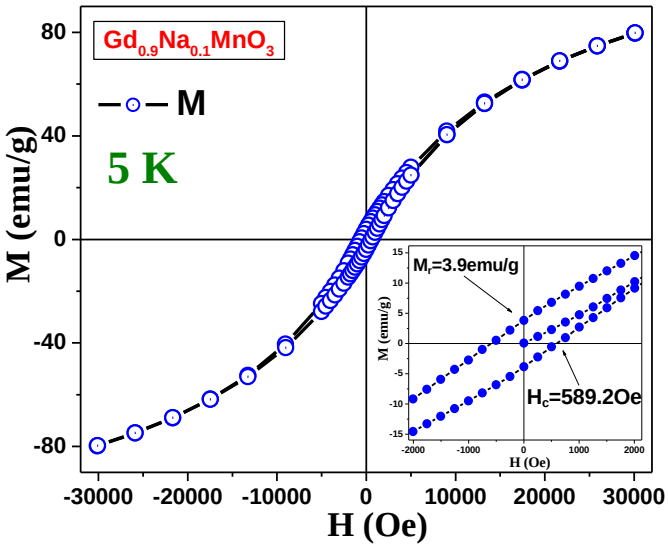

Fig. 15. M-H loop of $Gd_{0.9}Na_{0.1}MnO_3$ compound taken at 5K. Inset shows the enlarged hysteresis part of the loop.

Conclusion

Undoped $GdMnO_3$ and 10mol% Na-doped $Gd_{0.9}Na_{0.1}MnO_3$ tiny single crystals with orthorhombic perovskite structure are synthesized by the sol-gel route to study the effect of monovalent cation doping on structural, microstructural and magnetic properties of $GdMnO_3$. Tiny single crystals of ~ 200nm size are formed after 12 h sintering the compounds at 1000ºC. Microstructures of both compounds are characterized by the Rietveld refinement of the XRD patterns and analyzing respective HRTEM images. Elemental composition is verified from TEM-EDX spectra and the presence of Mn^{4+} along with Mn^{3+} valence state is confirmed from XPS analysis. Though both the compounds belong to an O´ orthorhombic phase, Na doping results into lattice contraction, decrease in unit cell volume, perovskite parameter and spontaneous strain indicating a better structural stability in the Na-doped compound. These

structural changes occur due to partial replacement of Gd^{+3} by Na^{+} and creation of Mn^{+4}. An increase in Goldschmidt tolerance factor and decrease in angular distortion indicates better stability of MnO_6 octahedra in Na doped compound. Both the lattice and octahedral distortions in $GdMnO_3$ are reduced due to Na doping. A reduction in Mn-O bond length indicates that the Jahn-Teller distortion is also reduced due to Na doping. The microstructural changes influence the magnetic properties of $GdMnO_3$ compound as the magnetic transition temperature increases and the ferromagnetic interaction strengthens due to Na doping. The Nèel temperature of $GdMnO_3$ is found out to be 44K whereas the Curie temperature of $Gd_{0.9}Na_{0.1}MnO_3$ is found out to be 51K. Magnetic hysteresis curve signifies dominant Gd spin ordering at 5K. Thus by adding only 10% Na, the microstructure and degree of lattice distortion can be controlled which in turn tunes the magnetic behavior of $GdMnO_3$ compound.

Acknowledgements

Authors (SKP & AN) wish to thank the UGC-DAE consortium for Scientific Research, Kolkata Centre for providing the SQUID facility. The UGC is acknowledged for providing grant (F.530/5/CAS/2011(SAP-I) dated 05.11.2011) towards research through the 'Centre of Advanced Study' in the identified thrust area 'condensed matter physics including laser application'. DST-FIST, Govt. of India is acknowledged for grant (SR/FST/PSI-170/2011 dated 18.05.2012) towards XRD.

References

1 Y. Tokura, Y. Tomioka, *J. Magn. Magn. Mater.* 1999, **200**, 1-23.

2 C. N. R. Rao, A. Arulraj, P. N. Santosh and A. K. Cheetham, *Chem. Mater.* 1998, **10**, 2714-2722.

3 C. N. R. Rao, A. Arulraj, A. K. Cheetham and B. Raveau, *J. Phys.: Condens. Matter* 2000, **12**, R83–R106.

4 Y. Tomioka, T. Okuda, Y. Okimoto, A. Asamitsu, H. Kuwahara and Y. Tokura, *J. Alloys Comp.* 2001, **326**, 27–35.

5 C.N.R. Rao and P.V. Vanitha, *Curr. Opin. Solid State Mater. Sci.* 2002, **6**, 97–106.

6 C. Moure and J. Pena, *J. Magn. Magn. Mater.* 2013, **337–338**, 1–22.

7 J. M. D. Coey, M. Viret and S. von Molnar, *Adv. Phy.* 1999, **48**, 167-293.

8 D. W. Visser and A. P. Ramirez, *Phys. Rev. Lett.* 1997, **78**, 3947-3950.

9 C.N.R. Rao and A.K. Raychaudhuri, *Colossal Magnetoresistance, Charge Ordering and related properties of Manganese Oxides*, ed. C.N.R. Rao, B. Raveau, World Scientific, Singapore, 2004, p 1-43.

10 P. G. Radaelli, M. Marezio, H. Y. Hwang, S-W. Cheong and B. Batlogg, *Phys. Rev. B* 1996, **54**, 8992-8995.

11 B. Dabrowski, S. Kolesnik, A. Baszczuk, O. Chmaissem, T. Maxwell and J. Mais, *J. Solid State chem.* 2005, **178**, 629–637.

12 R. Das, A. Jaiswal and P. Poddar, *J. Phys. D: Appl. Phys.* 2013, **46**, 045301 (7pp)

13 A. Pimenov, A.A. Mukhin, V. Yu Ivanov, V.D. Travkin, A.M. Balbashov and A. Loidl, *Nat. Phys.* **2006**, *2*, 97-100.

14 T. Arima, T. Goto, Y. Yamasaki, S. Miyasaka, K. Ishii, M. Tsubota, T. Inami, Y. Murakami and Y. Tokura, *Phys. Rev. B* 2005, **72**, 100102.

15 J. Baier, D. Meier, K. Berggold, J. Hemberger, A. Balbashov, J. A. Mydosh and T. Lorenz, *Phys. Rev. B* 2006, **73**, 100402.

16 W. S. Ferreira, J.A. Moreira, A. Almeida, M.R. Chaves, J.P. Araújo, J.B. Oliveira, J.M.M. Da Silva, M.A. Sá, T.M. Mendonca and P.S. Carvalho, *Phys. Rev. B* 2009, **79**, 054303.

17 X.L. Wang, D. Li, T.Y. Cui, P. Kharel, W. Liu and Z. D. Zhang, *J. Appl. Phys.* 2010, **107**, 09B510.

18 R. Feyerherm, E. Dudzik, A.U.B. Wolter, S. Valencia, O. Prokhnenko, A. Maljuk, S. Landsgesell, N. Aliouane, L. Bouchenoire, S. Brown and D.N. Argyriou, *Phys. Rev. B* 2009, **79**, 134426.

19 J. Hemberger, S. Lobina, H.A.K. von Nidda, N. Tristan, V. Yu. Ivanov, A.A. Mukhin, A. M. Balbashov and A. Loidl, *Phys. Rev. B* 2004, **70**, 024414.

20 S. Samantaray, D.K. Mishra, S.K. Pradhan, P. Mishra, B.R. Sekhar, D. Behera, P.P. Rout, S.K. Das, D.R. Sahu and B.K. Roul, *J. Magn. Magn. Mater.* 2013, **339**, 168–174.

21 J. Oliveira, J.A. Moreira, A. Almeida, V.H. Rodrigues, M.M.R. Costa, P. B. Tavares, P. Bouvier, M. Guennou and J. Kreisel, *Phys. Rev. B* 2012, **85**, 052101.

22 O. Pena, M. Bahout, K. Ghanimi, P. Duran, D. Gutierrez, C. Moure, *J. Mater. Chem.* 2002, **12**, 2480–2485.

23 B. Jaya Prakash, K. Naveen Kumar and S. Buddhudu, *Ferroelectr. Lett.* 2012, **39**, 104-116.

24 P. Negi, G. Dixit, H.M. Agrawal, R.C. Srivastava, *J. Supercond. Nov. Magn.* 2013, **26**, 1611–1615.

25 Y. Romaguera-Barcelay, J. Agostinho Moreira, A. Almeida, P.B. Tavares, J. Pérez de la Cruz, *Thin Solid Films* 2014, **564**, 419–425.

26 X. Li, C. Lu, J. Dai, S. Dong, Y. Chen, N. Hu, G. Wu, M. Liu, Z. Yan and J.M. Liu, *Sci. Rep.* 2014, **4**, 7019.

27 Y. Chen, H. Yuan, G. Li, G. Tian and S. Feng, *J. Cryst. Growth* 2007, **305**, 242–248.

28 T. Kimura, G. Lawes, T. Goto, Y. Tokura and A. P. Ramirez, *Phys. Rev. B* 2005, **71**, 224425.

29 T. Mori, N. Kamegashira, K. Aoki, T. Shishido and T. Fukuda, *Mater. Lett.* 2002, **54**, 238–243.

30 P.K. Siwach, H.K. Singh and O.N. Srivastava, *J. Phys.: Condens. Matter* 2008, **20**, 273201 (43pp).

31 C. Zener, *Phys. Rev.* 1951, **81**, 440-444.

32 R.M. Sarguna, V. Sridharan, S.S. Samatham, V. Ganesan, S. Bhardwaj, A.M. Awasthi, M. D. Mukadam, S. M. Yusuf, A.K. Sinha and N. Subramanian, *J. Phys.: Condens. Matter* 2014, **26**, 345901 (6pp)

33 A. Hirano, F. Hirano, T. Matsumura, N. Imanishi and Y. Takeda, *Solid State Ionics* 2006, **177**, 749–755.

34 S. Biswas, M.H. Khan, S. Pal and E. Bose, *J. Supercond. Nov. Magn.* 2014, **27**, 463-468.

35 A. Nandy, A. Roychowdhury, D. Das and S.K. Pradhan, *Powder Technol.* 2014, **254**, 538–547.

36 S. Bid and S. K. Pradhan, *J. Appl. Cryst.* 2002, **35**, 517-525.

37 R.A. Young, *The Rietveld Method*, ed. R. A. Young, IUCr/Oxford University Press, 1996, pp. 1–38.

38 L. Lutterotti, Maud Version 2.26, http://www.ing.unitn.it/_maud/ (accessed 13.07.2015)

39 H. M. Rietveld, *Acta Crystallogr.* 1967, **22**, 151–152.

40 H. M. Rietveld, *J. Appl. Crystallogr.* 1969, **2**, 65–71.

41 J. A. Alonso, M. J. Martinez-Lope, M. T. Casais and M.T. Fernandez-Diaz, *Inorg. Chem.* 2000, **39**, 917-923.

42 R. D. Shannon, *Acta Cryst. A* 1976, **32**, 751.

43 Y. Tadokoro, Y.J. Shan, T. Nakamura and S. Nakamura, *Solid State Ionics* 1998, **108**, 261–267.

44 J.B. Goodenough and J.M. Longo, *Magnetic and Other Properties in Oxides and Related Compounds*, ed. K.H. Hellwege, A.M. Hellwege, Springer-Verlag: Berlin, 1970, Group III, Vol. 4a, Chapter 3, p 126.

45 A. Nandy and S.K. Pradhan, *Dalton Trans.* **2015**, DOI: 10.1039/c5dt02154e

46 G.J. Snyder, C. H. Booth, F. Bridges, R. Hiskes, S. DiCarolis, M. R. Beasley and T. H. Geballe, *Phys. Rev. B* 1997, **55**, 6453-6459.

47 B. Samantaray, S.K. Srivastava and S. Ravi, *J. Magn. Magn. Mater.* 2011, **323**, 2622–2626.

48 H. Y. Hwang, S-W. Cheong, P. G. Radaelli, M. Marezio and B. Batlogg, *Phys. Rev. Lett.* 1995, **75**, 914-917.

For Table of Contents entry:

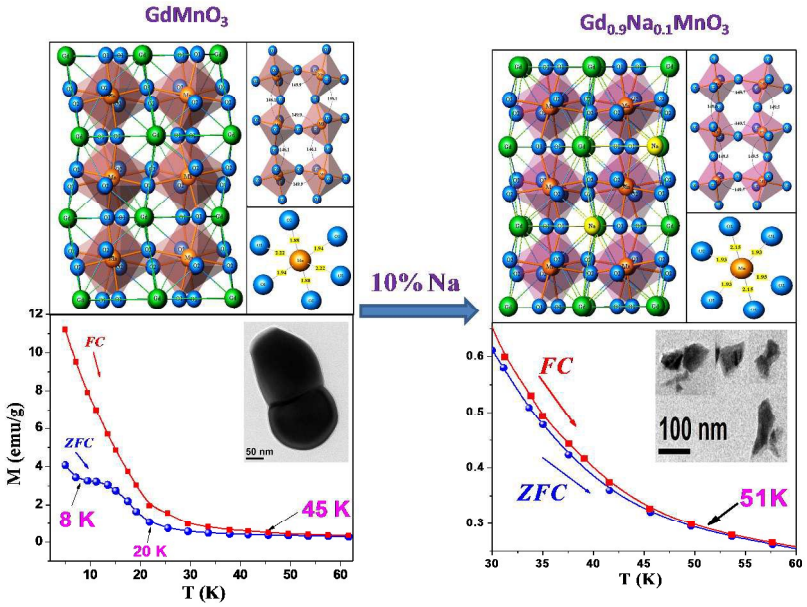

10% monovalent sodium doping reduces the octahedral and lattice distortion in $GdMnO_3$ tiny single crystals and introduces ferromagnetic ordering in the compound.